Chalcogenide Letters Vol. 19, No. 2, February 2022, p. 83 - 91

Synthesis of green phosphor $SrAl_2O_4$: Eu^{2+}, Dy^{3+}: Rietveld refinement and optical properties

N. N. N Roslan[a], W. A. W. Razali[a*], A. R. Tamuri[b], H. Azhan[a], Z. Mohamed[c]
[a]*Faculty of Applied Sciences, Universiti Teknologi MARA Pahang, 26400 Jengka, Pahang, Malaysia*
[b]*Department of Physics, Universiti Teknologi Malaysia, 81310 Skudai, Johor, Malaysia*
[c]*Faculty of Applied Sciences, Universiti Teknologi MARA, 40450 Shah Alam, Selangor, Malaysia*

Strontium aluminate ($SrAl_2O_4$), $SrAl_2O_4$: Eu^{2+} and $SrAl_2O_4$: Eu^{2+}/Dy^{3+} phosphors were prepared by solution combustion method. The XRD patterns of the sample were analysed using Rietveld refinement. The analysis confirmed the multiphase structure consisting of hexagonal ($P6_3$ space group) and monoclinic ($P12_1$ space group) phases. The refinement χ^2 values in the range of 2.1–2.8. The crystal structure model was generated based on the refined data. The refined unit cell volume show increment after Eu and Dy doping. The estimated crystallite size is approximately 19 nm and slightly increase after calcination. The emission spectra of the Eu^{2+} doped $SrAl_2O_4$ sample shows a broad emission band with a peak around 500 nm, corresponding to $4f^65d^1$–$4f^7$ transition. With additional Dy^{3+} doping, the emission peak shifted towards 522 nm, which emitted green light as illustrated by the CIE diagram. The synthesized compounds were also characterized by FTIR and UV-vis for their chemical bonding and energy band gap respectively.

(Received November 16, 2021; Accepted February 3, 2022)

Keywords: Strontium aluminate, Rare earth doping, Solution combustion, Phosphor, Luminescence

1. Introduction

Phosphors incorporated with lanthanide ions have been widely investigated due to the suitability of these materials in numerous applications, such as light sources, light emitting diodes (LEDs), colour displays, and bioimaging [1-3]. One of the well-known phosphor materials is strontium aluminate ($SrAl_2O_4$) doped lanthanide ions. This material has attracted considerable interest from researchers due to its excellent phosphorescence properties, including thermal and chemical stability, high quantum efficiencies and long luminescence lifetime [4-7]. Previously, zinc sulphide doped with Co, Cu, and Mn was considered as the main phosphorus material that could obtain long luminescence lifetime. Later, strontium aluminates become well known due to longer luminescence lifetime [8].

Various activators, including Eu^{2+}, Dy^{3+}, Er^{3+}, Tb^{3+}, and Nd^{3+}, have been used as doping agents to obtain the desired luminescence property [9-12]. Moreover, transition metal ions, including Mn^{2+}, Ni^{2+}, Cu^{2+}, and Zn^{2+}, have been incorporated for enhancing luminescence intensity [13]. Strontium aluminate doped Eu^{2+} has become notable as the material that can be applied in novel smart fabrics and persistent luminescent materials [14, 15]. The addition of Dy^{3+} in samples can improve the optical properties [16]. In this study, Eu, Dy co-doped $SrAl_2O_4$ phosphor synthesised using combustion method is reported. This study is essential to provide information on the synthesis method of $SrAl_2O_4$ phosphor material and investigate the effect of adding rare earth elements (Eu^{2+}, Dy^{3+}) on the structural and optical properties of $SrAl_2O_4$. Rietveld refinement was carried out to carefully analyse the structural properties of the prepared sample. To the best of the

* Corresponding author: wanaizuddin@uitm.edu.my
https://doi.org/10.15251/CL.2022.192.83

authors knowledge, Rietveld refinement has not been fully reported for $SrAl_2O_4$ samples in other published literature. The optical properties of prepared $SrAl_2O_4$: Eu^{2+}, Dy^{3+} phosphor powder were investigated using photoluminescence (PL) analysis and ultraviolet-visible (UV-vis) spectroscopy. Meanwhile, the structural and chemical bond properties were analysed using X-ray diffraction (XRD) and Fourier transform infrared (FTIR) spectroscopy, respectively. This study would provide additional knowledge on the structural and optical analysis of $SrAl_2O_4$: Eu^{2+}, Dy^{3+} phosphor.

2. Experimental procedure

2.1. Sample synthesis

Stoichiometric amount of $Sr(NO_3)_2$ (99.5%, QReC), $Al(NO_3)_3 \cdot 9H_2O$ (98.9%, Sigma-Aldrich), Eu_2O_3 (99.9%) Huizhou GL Tech. Co. Ltd, Dy_2O_3 (99.9%) Huizhou GL Tech. Co. Ltd, and urea ($(NH_2)_2CO$) Bendosen 99.8% were prepared to synthesise $SrAl_2O_4$: Eu^{2+}, Dy^{3+} phosphor. 1 M of 65% nitric acid (HNO_3) was added to Eu_2O_3 and Dy_2O_3 to form $Eu(NO_3)_3$ and $Dy(NO_3)_3$, respectively. The conversion of these rare earth compounds into nitrate form. Then, $Eu(NO_3)_3$ and $Dy(NO_3)_3$ were mixed with $Sr(NO_3)_2$, $Al(NO_3)_3 \cdot 9H_2O$, and $(NH_2)_2CO$. Next, the solution was stirred for 2 h at 200 rpm and 70 °C using a magnetic stirrer. After that, the solution was transferred into an alumina crucible, placed in a preheated furnace, and maintained at 600 °C. At first, the solution was boiled to remove water, followed by decomposition under the existence of a large amount of gases. Later, the reagent immediately combusted and generated foamy and voluminous ash. The mixture becomes foam, which breaks with a flame and burns to incandescence. This process occurred about 9 min until completion. Afterwards, the crucible was removed and cooled to room temperature. The sample was ground into powder form using an agate mortar and pestle. For calcination, the sample was heated at 1,100 °C for 1.5 h.

2.2. Sample characterization

XRD patterns of the samples were collected using a Rigaku AX-2500 Advance X-ray spectrometer with Cu-Kα radiation (λ = 0.154 nm). The General Structure Analysis System (GSAS) with graphical user interface (EXPGUI), and visualisation for electronic structural analysis (VESTA) software were employed for structural refinement and to visualize the refined structure of compounds, respectively. A Perkin Elmer Spectrum 100 FTIR spectrometer with attenuated total reflection (ATR) mode in the range of 4500–400 cm^{-1} was used to record the sample's IR absorption spectra. The PL was measured using a Horiba Fluoromax-4 spectrofluorometer in the range of 400–700 nm. The absorption spectra were obtained using a Shimadzu UV-1800 UV-vis spectrometer in the range of 200–1,100 nm.

The crystallite size was calculated using the Debye-Scherrer equation:

$$D = k\lambda/\beta \cos\theta \quad (1)$$

where D is the average crystal size, k is the Scherrer constant (i.e., 0.90), β is the full at half maximum, and θ is the diffraction angle.

The energy band gap can be calculated using the Tauc relation:

$$(\alpha h\upsilon)^2 = K^2 (h\upsilon - Eg) \quad (2)$$

where α is the coefficient of absorption, $h\upsilon$ is the energy of photon, K is fixed depending on the form of transition, and E_g is the band gap. The band gap energy can be estimated by plotting $(\alpha h\upsilon)^2$ against $h\upsilon$ and extending the linear region of the graph to $(\alpha h\upsilon)^2 = 0$. The intersection point of the line at the x-axis is the band gap value.

3. Results and discussion

The XRD pattern of undoped $SrAl_2O_4$ before and after calcination is shown in Figure 1(a). After calcination, it can be seen that the peak becomes narrower, and the intensity increases. From the XRD patterns in Figure 1(b), all spectra contain intense and sharp peaks, indicating high crystallinity. All the peaks matched well with the Joint Committee on Powder Diffraction Standard (JCPDS) No. 34-0379, confirming that the samples are $SrAl_2O_4$. The spectra were further analysed with Rietveld refinement. The refined XRD results are shown in Figure 1(c–d). The solid black line shows the Rietveld refinement, whereas the red + point is the measured XRD spectra. The quality of the Rietveld refinement is estimated in terms of the weighted profile R-factor (R_{wp}), unweighted profile R factor (R_p), and chi-squared (χ^2), as listed in Table 1. Table 1 also lists the crystallographic parameters extracted from the Rietveld refinement of the corresponding XRD spectra. From the results, it is observed that the samples contain multiphase structures, which are consistent with previous findings [4]. The formation of these structures depends on the heat treatment during sample preparation, whereby a monoclinic phase is formed at low temperatures and a hexagonal phase is formed at high temperatures [17-19]. A hexagonal structure typically forms at the transition temperature of 650 °C [18]. Based on the analysis, it is confirmed that the main phase present in the samples is the hexagonal phase with $P6_3$ space group (shown as a red tick vertical line in Figure 1(c–d)).

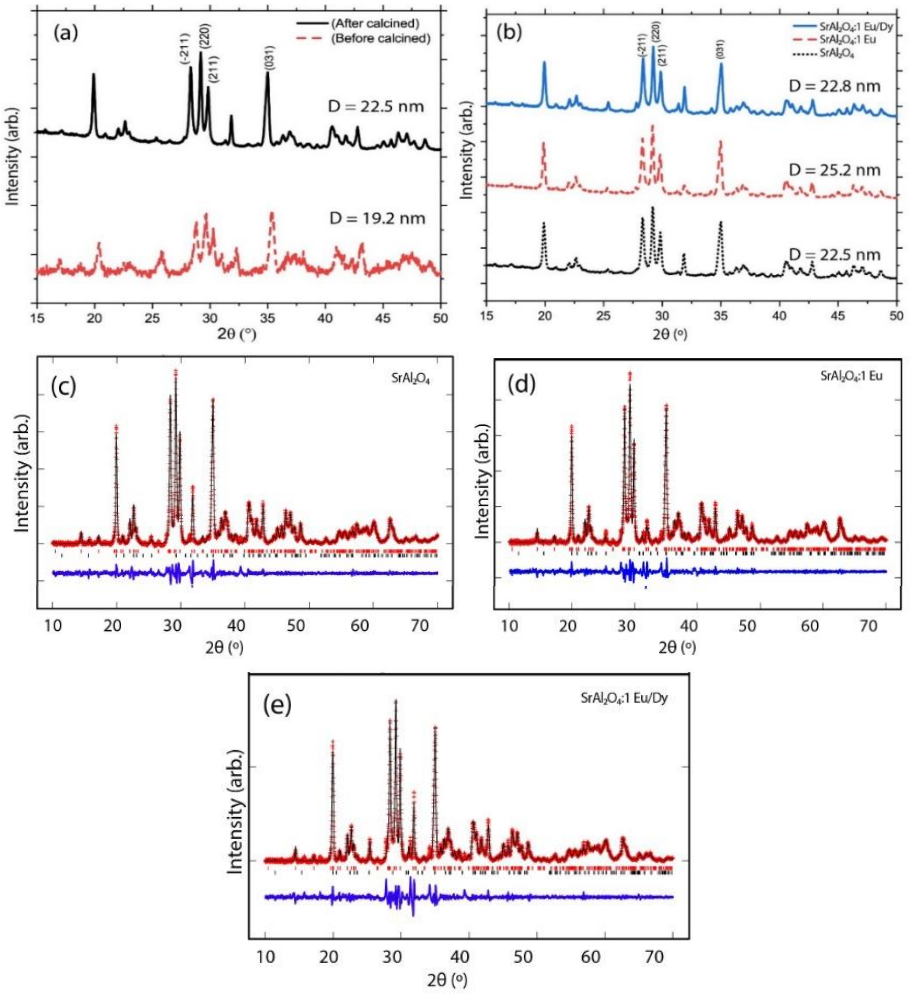

Fig. 1. a) XRD pattern for undoped $SrAl_2O_4$ before (black solid line) and after calcined (red dash line). b) XRD pattern for $SrAl_2O_4$, Eu^{2+} doped $SrAl_2O_4$ (1.0 mol%) and Eu^{2+}, Dy^{3+} co-doped $SrAl_2O_4$ (1.0 mol %) phosphors after calcination. Rietveld refinements of XRD patterns for (c) undoped, (d) Eu^{2+} doped and (e) Dy^{3+} doped. Observed (red +), calculated (black line) and difference between

observed and calculated (blue line). First and second detected phases are denoted by red and black tick vertical lines respectively.

Meanwhile, another phase detected is the monoclinic phase material with $P12_1$ space group (shown as a black tick vertical line in Figure 1(c–d)). The refined hexagonal and monoclinic phases generated using Vesta software are shown in Figure 2. The lattice parameters agreed well with published data [20, 21]. It is found that the lattice parameter c for doped samples is slightly larger than the undoped sample. The refined lattice angles for all samples are $\alpha = \beta = 90°$ and $\gamma = 120°$. The refined unit cell volume (V) increased after the sample had been doped with Eu and Dy, implying that the addition of other elements increases the cell volume. The χ^2 values in the range of 2.1–2.8 show a good refinement result considering the samples have multiphase structures. It is also observed that some of the XRD data did not fit well, indicating the presence of impurities in the sample, which might be due to unreacted chemicals present in the sample. The crystallite size of the undoped sample is stated in Figure 1(a). The crystallite size after calcination increased from 19.2 nm to 22.5 nm. The increment is likely due to crystallite growth by the thermal effect [22]. The crystallite sizes of undoped $SrAl_2O_4$, $SrAl_2O_4$: Eu^{2+}, and $SrAl_2O_4$: Eu^{2+}/Dy^{3+} are 22.5 nm, 25.2 nm, and 22.8 nm, respectively. From Figure 1(b), the sample doped with Eu^{2+} has the biggest crystallite size. However, the size becomes smaller for Dy^{3+}, Eu^{2+} co-doped $SrAl_2O_4$ sample. The difference in crystallite size is probably due to differences in ionic radius [23].

Table 1. Lattice parameters, unit cell volume, and fit goodness (χ^2) in $SrAl_2O_4$ (doped and undoped) as obtained from Rietveld refinement.

Sample	**$SrAl_2O_4$**	**Eu:$SrAl_2O_4$**	**Dy/Eu: $SrAl_2O_4$**
Space group	$P6_3$	$P6_3$	$P6_3$
	hexagonal	hexagonal	hexagonal
a (Å)	8.8567(5)	8.8476(5)	8.8697(3)
b (Å)	8.8567(5)	8.8476(5)	8.8697(4)
c (Å)	8.3804(7)	8.6632(7)	8.6531(4)
α=β **γ** **Volume(Å^3)**	90.0 120.0 569.308(3)	90.0 120.0 587.314(3)	90.0 120.0 589.564(2)
R_P(%)	11.42	12.64	10.69
R_{WP}(%)	14.21	16.32	17.31
χ2	2.817	2.065	2.241

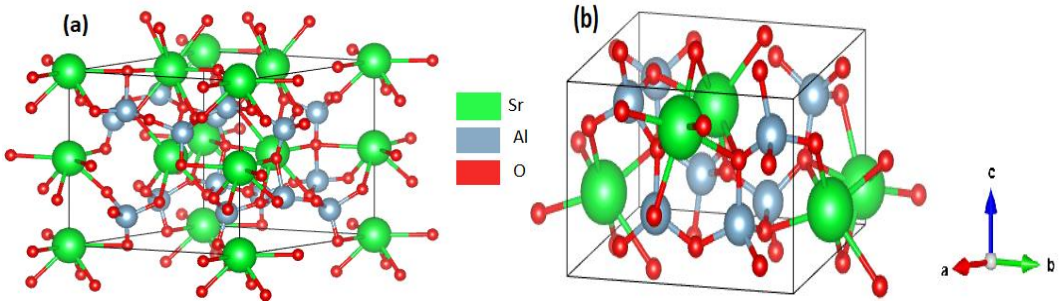

Fig. 2. (a) Refined hexagonal phase (P63 space group) and (b) monoclinic (P121 space group) generated using Vesta software.

The results of FTIR analysis for $SrAl_2O_4$, $SrAl_2O_4$: Eu^{2+}, and $SrAl_2O_4$: Eu^{2+}/Dy^{3+} are shown in Figure 3. Based on the results, all the samples show a peak at 3750 cm^{-1}, which is due to N-H stretching vibration. This peak likely originates from nitrates present in the starting material [24]. A broad band observed at 3454 cm^{-1} is caused by the O-H stretching vibration of free and

hydrogen-bonded hydroxyl groups. The presence of this broad band is due to the humidity level in the air [25]. Next, the peak appearing in the region of 1712 cm^{-1} is due to C-O vibration. The presence of a very weak band in 1360 cm^{-1} is from the symmetric stretching of N-O group vibration, which could originate from nitrates in the raw material [26]. Another peak found at 742 cm^{-1} is caused by the stretching of Sr-O vibration. Furthermore, the symmetric bonding of O-Al-O is discovered at 437 cm^{-1}. The FTIR results are summarised in Table 2.

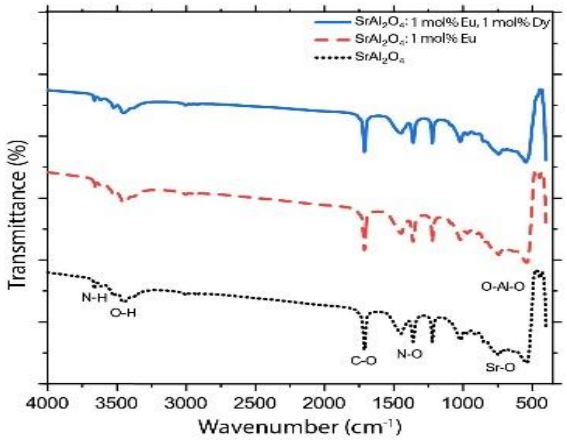

Fig. 3. FTIR Spectra of $SrAl_2O_4$, $SrAl_2O_4$: 1 mol% Eu^{2+} and $SrAl_2O_4$: 1 mol% Eu^{2+}, 1 mol% Dy^{3+} phosphor powder

Table 2. FTIR analysis of $SrAl_2O_4$, $SrAl_2O_4$: 1 mol% Eu^{2+} and $SrAl_2O_4$: 1 mol% Eu^{2+}, 1 mol% Dy^{3+} phosphor powder.

Absorption peaks (cm^{-1})	**Assignments**
3750 3454	N-H stretching vibrations O-H stretching vibrations
1712	C=O vibrations
1360	N-O stretching vibrations
742	Sr-O stretching vibrations
437	O-Al-O symmetric stretching

PL analysis was conducted to analyse the luminescence properties of Eu^{2+} doped $SrAl_2O_4$ and Dy^{3+}, Eu^{2+} co-doped $SrAl_2O_4$. Figure 4 shows the emission spectra of Eu^{2+} doped $SrAl_2O_4$ and Dy^{3+}, Eu^{2+} co-doped $SrAl_2O_4$ identified in the range of 400–700 nm under the UV excitation at 337 nm. The emission spectra of Eu^{2+} doped $SrAl_2O_4$ sample show a broad emission band with a peak at 500 nm. This emission corresponds to $4f^65d^1 – 4f^7$ transition [27]. From the analysis, the sample with 1 mol % Eu^{2+} concentration shows the highest emission intensity. Thus, this Eu^{2+} concentration was used for preparing Dy^{3+}, Eu^{2+} co-doped $SrAl_2O_4$ sample. The emission peak Eu^{2+}, Dy^{3+} co-doped $SrAl_2O_4$ is at 507 nm and shifted to 525 nm with the increase of Dy^{3+} concentration. The higher Dy^{3+}concentration results in a larger shift. This shift might be due to the changes of the crystal lattice around Eu^{2+} and the quantum size effect of the phosphor [28]. The addition of Dy^{3+} did not show its characteristic emission but is likely to transfer the absorbed energy into the host matrix of Eu^{2+} ions. The Eu^{2+} ions are predicted to substitute Sr sites with similar crystallographic arrangement [29]. Dy^{3+} can activate hole trap levels to extend the afterglow. The valence electrons of Eu^{2+} captured by Dy^{3+} donated traps can be released gradually and recombined under thermal re-excitation with the excited state of Eu^{2+} and then returned to the ground state of Eu^{2+}, accompanied by green light emission. This process will result in long afterglow. Therefore, more hole trap levels are created in $SrAl_2O_4$: Eu^{2+} samples with higher Dy^{3+}

concentrations, leading to higher PL intensities [30]. Figure 5 displays the Commission International de L'Echairage (CIE) 1931 coordinates for Eu^{2+}, Dy^{3+} co-doped $SrAl_2O_4$ excited at 337 nm. The chromaticity coordinate for green light is located at (0.2866, 0.5475) [31]. The emission of $SrAl_2O_4$: Eu^{2+}, Dy^{3+} is confirmed in the green region with coordinate (0.27685, 0.57518) of the colour space after calculation using the colour coordinate.

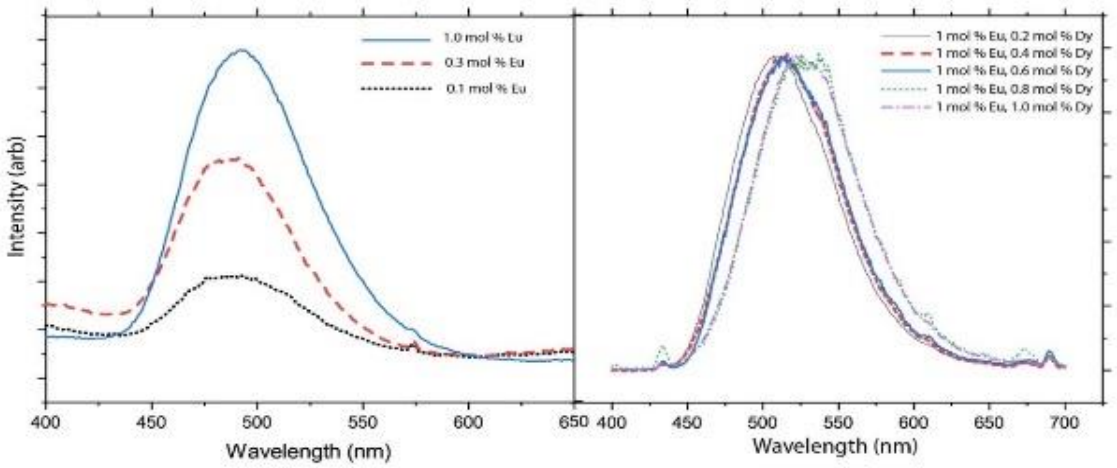

Fig. 4. PL emission spectra of samples $SrAl_2O_4$: Eu^{2+}, with 0.1, 0.3, 1.0 mol% concentration of Eu^{2+} (left) and $SrAl_2O_4$: Eu^{2+}/Dy^{3+} with 1.0 mol% concentration of Eu^{2+} and 0.2, 0.4, 0.6, 0.8, 1.0 mol% concentration of Dy^{3+} (right), excited at 337 nm wavelength radiation.

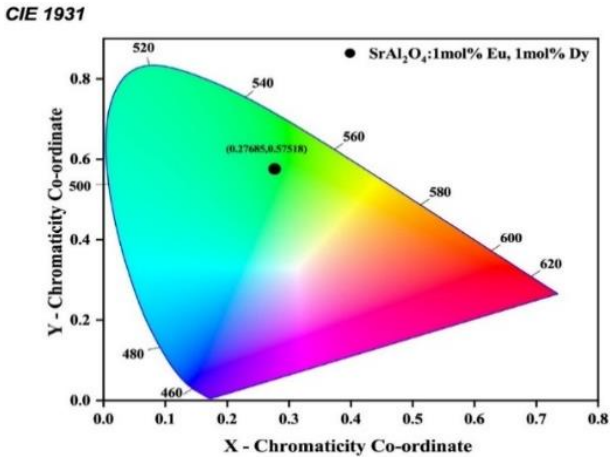

Fig. 5. CIE plot coordinates of $SrAl_2O_4$:1 mol% Eu^{2+}, 1 mol% Dy^{3+}.

Based on Figure 6(a), the doped samples have almost the same spectrum as the undoped sample due to the small percentage of rare earth used for each sample. The spectra have a strong absorption band at 200 nm, followed by a weak broad band in the region of 240–600 nm. No absorption band was observed after 600 nm. The weak bands observed are due to the structural defects in $SrAl_2O_4$ phosphor powder. The absorbance of the sample doped with Eu^{2+} and Dy^{3+} is slightly higher than the undoped sample. This might be caused by the increased absorption of photon energy at longer wavelengths from the reduction in band gap [32]. Figure 6(b) shows the Tauc plots for the energy band gap of undoped $SrAl_2O_4$, Eu^{2+} doped $SrAl_2O_4$, and Eu^{2+}, Dy^{3+}co-doped $SrAl_2O_4$. The absorption can be considered as a direct band gap as it does not require phonon during photon emission. From the graph, the band gap energy values for undoped $SrAl_2O_4$, Eu^{2+} doped $SrAl_2O_4$, and Dy^{3+}, Eu^{2+} co-doped $SrAl_2O_4$ are 5.4264 eV, 5.3162 eV, and 5.4168 eV,

respectively. The band gap decreases after doping $SrAl_2O_4$ with Eu^{2+} and Dy^{3+}. The decrease of band gap is likely due to the localised rate of defects caused by the doping of Eu^{2+} and Dy^{3+} ions within the $SrAl_2O_4$ host band gap. Ionic radii are vital in the decrease of band gap. The ionic radii for Sr^{2+}, Eu^{2+}, and Dy^{3+} are 0.127 nm, 0.13 nm, and 0.091 nm, respectively. As the ionic radius of Eu^{2+} is higher than Sr^{2+}, it replaced Sr^{2+} in $SrAl_2O_4$. The difference in ionic radii causes lattice expansion in $SrAl_2O_4$. There is not much difference in the band gap after doping with Dy^{3+} as the ionic radius of Dy^{3+} and Sr^{2+} is almost similar [32].

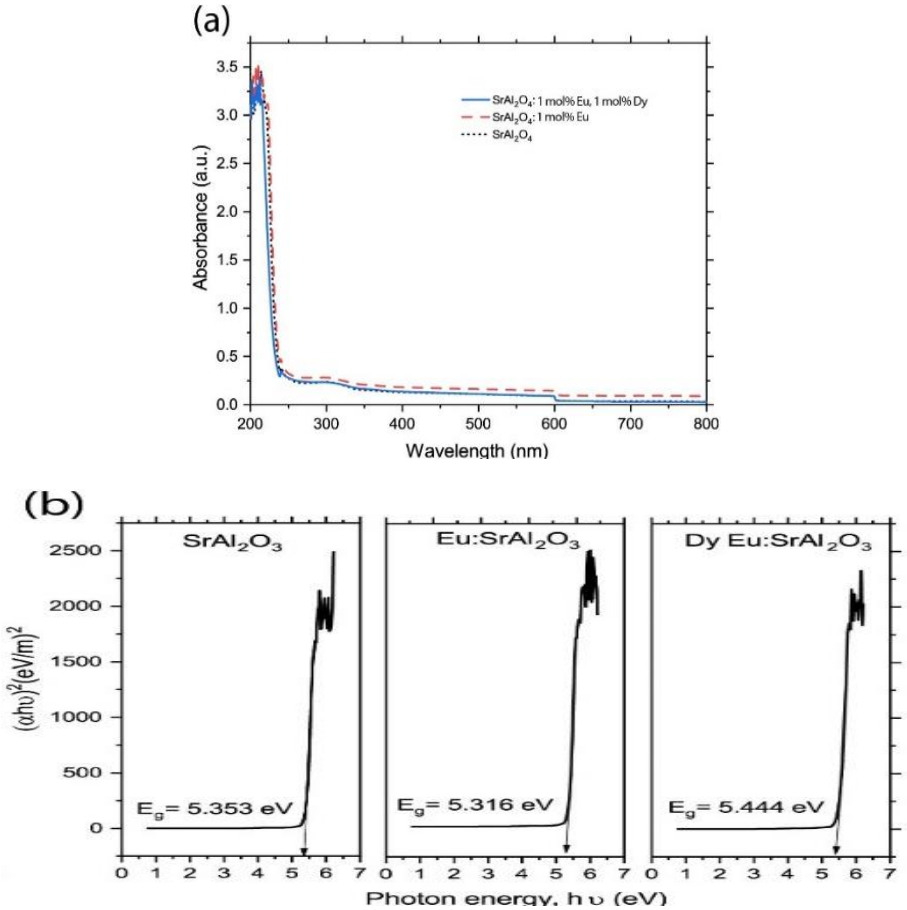

Fig. 6. (a) UV-vis Absorption spectra for $SrAl_2O_4$, 1 mol% Eu^{2+} doped $SrAl_2O_4$, 1 mol% Dy^{3+}, 1 mol% Eu^{2+} co-doped $SrAl_2O_4$ phosphors (b) Tauc plot for energy band gap estimation calculated from absorption spectra of a) $SrAl_2O_4$, b) $SrAl_2O_4$: Eu^{2+} and c) $SrAl_2O_4$: Eu^{2+}/Dy^{3+}.

4. Conclusion

Undoped $SrAl_2O_4$, Eu^{2+} doped $SrAl_2O_4$, and Eu^{2+}, Dy^{3+} co-doped $SrAl_2O_4$ were successfully synthesised using the solution combustion method. The XRD patterns were analysed using Rietveld refinement with χ^2 values in the range of 2.1–2.8. Based on the analysis, it is confirmed that the main phase is hexagonal with $P6_3$ space group. While another phase is monoclinic with $P12_1$ space group. The crystallite size was found between 19 to 25 nm. The PL analysis reveals that the sample produce broad emission band which corresponds to $4f^65d^1 - 4f^7$ transition. For the Dy^{3+}, Eu^{2+} co-doped $SrAl_2O_4$ sample, the emission peaks slightly shifted towards longer wavelength. CIE plots proved that this peak exhibit green emission which potentially can be applied as a green phosphor for green LEDs.

Acknowledgments

The author would like to acknowledge the Ministry of Higher Education Malaysia for financial support via Fundamental Research Grant Scheme (FRGS) No. 600-IRMI/FRGS 5/3 (266/2019). We acknowledge Universiti Teknologi MARA and Universiti Teknologi Malaysia for their research facilities.

References

[1] Y. Jiang, J. Huang, X. Zhen, Z. Zeng, J. Li, C. Xie, Q. Miao, J. Chen, P. Chen, K. Pu, Nature communications 10, 1 (2019).; https://doi.org/10.1038/s41467-019-10119-x

[2] T. Lecuyer, E. Teston, G. Ramirez-Garcia, T. Maldiney, B. Viana, J. Seguin, N. Mignet,D. Scherman, C. Richard, Theranostics 6, 2488 (2016); https://doi.org/10.7150/thno.16589

[3] A. R. Camacho, F. C. Romo, A. G. Murillo, J. O. Uc, Journal of the Australian Ceramic Society 56, 447 (2020); https://doi.org/10.1007/s41779-019-00348-0

[4] R. E. Rojas-Hernandez, F. Rubio-Marcos, A. Serrano, A. Rakhmatullin, C. Bessada, J. F. Fernandez, RSC advances 8, 28918 (2018); https://doi.org/10.1039/C8RA05601C

[5] D. Kshatri, A. Khare, P. Jha, Chalcogenide Lett 10, 121 (2013)

[6] A. N. Bone, A Report of a Senior Study, Maryville College, (2017).

[7] J. Montes-Frausto, K. Juarez-Moreno, B. Can-Uc, G. Hirata-Flores, Optical Materials Express 6, 1488 (2016); https://doi.org/10.1364/OME.6.001488

[8] I. Bite, G. Krieke, A. Zolotarjovs, K. Laganovska, V. Liepina, K. Smits, K. Auzins, L. Grigorjeva, D. Millers, L. Skuja, Materials & Design 160, 794 (2018); https://doi.org/10.1016/j.matdes.2018.10.021

[9] H. Deng, D. Chen, Chalcogenide Letters 18, 617 (2021).

[10] V. Havasi, D. Tátrai, G. Szabó, E. Varga, A. Erdőhelyi, G. Sipos, Z. Kónya, A. Kukovecz, Journal of Luminescence 219, 116917 (2020); https://doi.org/10.1016/j.jlumin.2019.116917

[11] Y. Chen, K. Zhang, X. Wang, Y. Bao, Journal of the Australian Ceramic Society 53, 993 (2017); https://doi.org/10.1007/s41779-017-0116-9

[12] X. Zhang, L. Wang, Chalcogenide Lett 12, 435 (2015); https://doi.org/10.2174/1570162X1206150311161529

[13] X. Hu, L. Wu, H. Yin, G. Li, D. Guo, Journal of Materials Science: Materials in Electronics 30, 3804 (2019); https://doi.org/10.1007/s10854-019-00664-y

[14] T. A. Khattab, M. Rehan, Y. Hamdy, T. I. Shaheen, Industrial & Engineering Chemistry Research 57, 11483 (2018); https://doi.org/10.1021/acs.iecr.8b01594

[15] D. Dutczak, T. Jüstel, C. Ronda, A. Meijerink, Physical Chemistry Chemical Physics 17, 15236 (2015); https://doi.org/10.1039/C5CP01095K

[16] H. Wang, X. Liang, K. Liu, Q. Zhou, P. Chen, J. Wang, J. Li, Optical Materials 53, 94 (2016); https://doi.org/10.1016/j.optmat.2016.01.030

[17] R. Wiglusz, T. Grzyb, A. Watras, P. Deren, S. Lis, W. Strek, Journal of Rare Earths 29, 1105 (2011); https://doi.org/10.1016/S1002-0721(10)60607-2

[18] R. Zhang, G. Han, L. Zhang, B. Yang, Materials Chemistry and Physics 113, 255 (2009); https://doi.org/10.1016/j.matchemphys.2008.07.085

[19] K. Gedekar, S. Wankhede, S. Moharil, R. Belekar, Journal of Advanced Ceramics 6, 341 (2017).

[20] M. V. D. S. Rezende, A. Andrade, M. E. Valerio, P. J. R. Montes, Journal of Applied Physics 115, 103510 (2014); https://doi.org/10.1063/1.4868470

[21] K. Fukuda, K. Fukushima, Journal of Solid State Chemistry 178, 2709 (2005); https://doi.org/10.1016/j.jssc.2005.06.012

[22] Y.-F. Chen, C.-Y. Lee, M.-Y. Yeng, H.-T. Chiu, Journal of crystal growth 247, 363 (2003); https://doi.org/10.1016/S0022-0248(02)01938-3

[23] P. D. C. Seta, P. E. Yunita, M. A. Baqiya, IOP Conference Series: Materials Science and Engineering, 196,1 (2017)

[24] B. Stuart, Infrared Spectroscopy: Fundamentals and Applications. (John Wiley & Sons, Ltd, 2004); https://doi.org/10.1002/0470011149

[25] A. Kumar, G. Kedawat, P. Kumar, J. Dwivedi, B. K. Gupta, New Journal of Chemistry 39, 3380 (2015); https://doi.org/10.1039/C4NJ02333A

[26] D. Bisen, R. Sharma, Luminescence 31, 394 (2016); https://doi.org/10.1002/bio.2972

[27] T. Peng, H. Yang, X. Pu, B. Hu, Z. Jiang, C. Yan, Materials letters 58, 352 (2004); https://doi.org/10.1016/S0167-577X(03)00499-3

[28] D. Kshatri, A. Khare, P. Jha, Optik-International Journal for Light and Electron Optics 124, 2974 (2013); https://doi.org/10.1016/j.ijleo.2012.09.045

[29] S. A. Pardhi, G. B. Nair, R. Sharma, S. Dhoble, Journal of Luminescence 187, 492 (2017); https://doi.org/10.1016/j.jlumin.2017.03.028

[30] I. P. Sahu, D. Bisen, R. Sharma, Research on Chemical Intermediates 42, 2791 (2016); https://doi.org/10.1007/s11164-015-2177-0

[31] H. Terraschke, M. Suta, M. Adlung, S. Mammadova, N. Musayeva, R. Jabbarov, M. Nazarov, C. Wickleder, Journal of Spectroscopy 2015 (2015); https://doi.org/10.1155/2015/541958

[32] M. M. Colen, Doctor of Philosophy thesis, Saga University, (2015).